EFFECT OF TARGET MATERIAL YIELD STRENGTH ON HYPERVELOCITY PERFORATION AND BALLISTIC LIMIT

Robert G. Thomson and E. T. Kruszewski

NASA Langley Research Center
Langley Station, Hampton, Va.

Presented at the 7th Hypervelocity Impact Symposium

Tampa, Florida
November 17-19, 1964

ABSTRACT 33369

A visco-plastic flow theory for the solution of hypervelocity perforation of thin plates has been investigated. A short time analytical solution including the effects of target material yield strength on perforation radii and ballistic limits was obtained. Expressions were derived for the velocities, displacements, strains, and strain rates present in the target material during hypervelocity impact. Pertinent parameters were varied and a comparison was made with the solution in which the yield strength was taken to be zero. The effect of target material yield strength was not found to be significant and resulted in little variation in the computed perforation radii.

Ballistic limit studies were also performed in which minimum plate thicknesses necessary to prevent perforation were established for projectiles of various masses, radii, and impacting velocities. Yield strength considerations were found to be of secondary importance; the more critical effect being produced by the projectile aspect ratio at impact.

AUTHOR

[redacted]

INTRODUCTION

An analytical solution to the problem of a rigid circular cylindrical projectile of finite mass impacting upon an infinite plate is presented in which yield strength considerations have been included in the governing equations. The results of reference 1 have been extended and, in addition, ballistic limits of thin plates have been determined. For the sake of completeness, the solution which was presented in reference 1 has been repeated in the appendix.

In references 2 and 3 an analytical solution was obtained for a problem similar to that of reference 1 except that the yield strength of the target plate was taken to be zero in the governing equations. A nonzero yield strength of the target material was introduced subsequently only to establish a separation criterion for perforation. An approximate two-dimensional analysis of the plate perforation problem (as stated in ref. 2) is presented in reference 4. This solution indicates that the radial velocities are about one order of magnitude less than the axial velocities and thus helps to justify the use of a one-dimensional approach.

An extension of the work presented in references 2 and 3 is given in reference 5, in which an attempt was made to include the effects of target material yield strength in the governing differential equation and associated boundary conditions. The results of the analysis are given in finite

series form and a parametric study is presented in which the effects of variations in the pertinent parameters on the radius of perforation are determined. Certain objections can be raised, however, to the results of reference 5. The expressions for velocity, displacement, strain, and strain rate presented in reference 5 do not correspond to the results presented earlier in references 2 and 3 as expected when the yield strength is taken to be zero. Furthermore, the solution of reference 5 yields the erroneous result that for the limiting case of an infinite mass projectile the velocity of the projectile decreases after impact. These considerations have provided the motivation for the present analysis.

The present solution agrees with the solution presented in references 2 and 3, in the limiting case when the yield strength is set equal to zero. In addition, the expression for velocity limits properly, for the case of the infinite mass projectile, to the condition that the velocity of the projectile remains constant after impact. The solution of reference 5, when compared with the present solution, is shown to contain additional mass ratio terms not found in the present solution.

The present report compares results obtained by including yield strength in the analysis with the results obtained for the same conditions when yield strength is taken to be zero. Some pertinent parameters such as initial velocity, mass, and radius of the impacting projectile as well as the target plate

thickness, yield strength, and viscosity are varied in order to study their effects on the radius of perforation. The ballistic limits of thin target plates are investigated as well and the importance of yield strength considerations is ascertained.

The ballistic limit studies determine the minimum target plate thicknesses necessary to prevent perforation. Ballistic limits are obtained for various values of target plate thickness and projectile mass, velocity, and radius.

SYMBOLS

The units used for the physical quantities defined in this paper are given both in the International System of Units (SI) and in the U.S. Customary Units. Factors relating the two systems are given in reference 14.

a	radius of projectile
C_1	dynamic ultimate yield strain in shear
g_o	initial projectile velocity
h	plate thickness
ζ	$2\pi ah/M$
H	$2\pi a^2 h\rho/M$
$i^n\text{erfc } x$	nth integral of erfc x (See appendix, eq. (A38))
I_n	modified Bessel function of first kind of order n
J_n	Bessel function of first kind of order n
k	dynamic yield stress in shear
K	$ka/V_o\mu$, Bingham number
K_n	modified Bessel function of second kind of order n
M_1	mass of projectile

M	mass of projectile and plug of plate material of radius a, $M_1 + \pi a^2 h\rho$
r	radial distance
$\bar{r}$	nondimensional radial distance, r/a
s	transform parameter
S_n	Struve function of order n
t	time
$\bar{t}$	nondimensional time, $\frac{\nu}{a^2} t$
V	axial velocity
$\bar{V}$	transform of V
V_o	initial velocity of projectile and target plug of radius a, $V_o = g_o \frac{M_1}{M}$
$\frac{V}{V_o}$	nondimensional velocity
$\frac{\partial \dot{W}}{\partial r} \frac{a}{V_o}$	nondimensional shear strain rate
w	axial displacement
$w \frac{\nu}{a^2 V_o}$	nondimensional displacement
$\frac{\partial W}{\partial r} \frac{\nu}{a V_o}$	nondimensional shear strain
Y_n	Bessel function of second kind of order n
γ	shear strain, $\frac{\partial w}{\partial r}$
μ	coefficient of dynamic viscosity
ν	coefficient of kinematic viscosity, $\frac{\mu}{\rho}$
ρ	mass density of plate material
τ_{rz}	transverse shear stress
z	axial coordinate

Subscripts:

cr critical

p perforation

A dot over a symbol denotes differentiation with respect to time t.

ANALYSIS

Governing Equations

In the present analysis, a rigid circular cylindrical projectile is considered to impact upon a thin infinite plate. The resulting perforation of the plate by the projectile is assumed to be a simple shear plugging perforation, in which only the transverse shear stresses act to resist the inertia of the impacting projectile. The perforation is also considered to be axially symmetric and the shear stress is taken to be constant through the thickness of the plate. The resulting deformations w of the plate are then represented as functions only of the radial coordinate r and the time t being independent of both the axial coordinate z and the circumferential coordinate θ. (See fig. 1(a).) Hence, by summing the forces in the axial direction on a circular ring element of plate material (see fig. 1(b)) the basic equation of motion for this simple shear perforation model can be written as

$$\frac{\partial \tau_{rz}}{\partial r} + \frac{\tau_{rz}}{r} = \rho \frac{\partial^2 w}{\partial t^2} \tag{1}$$

This approach and the following discussion on plate material and governing equations is similar to that presented in references 1, 2, 3, and 6.

The plate material considered herein is assumed to behave like an incompressible, visco-plastic Bingham solid in which the deformation accompanying transverse shearing commences only after the dynamic yield strength of the material has been reached. (See ref. 7.) When the value of the transverse shear stress falls below the yield strength of the material (or when the local rate of deformation becomes equal to zero), visco-plastic flow ceases and the material is assumed to be rigid in that region. The relation between the shear strain rate and shearing stress for the case of simple shear perforation can be written as (see ref. 7):

$$\tau_{rz} = \mu \frac{\partial \dot{w}}{\partial r} + \left(\text{sign } \frac{\partial \dot{w}}{\partial r}\right)k \qquad (2a)$$

or, since the sign $\partial \dot{w}/\partial r$ is always negative in this case

$$\tau_{rz} = \mu \frac{\partial \dot{w}}{\partial r} - k \qquad (2b)$$

where

μ dynamic viscosity of target material

k dynamic yield strength in shear of target material

$\frac{\partial \dot{w}}{\partial r} = \frac{\partial V}{\partial r}$ shear strain rate

and the relations between the velocity V, axial displacement w, and shear strain γ are

$V = \dot{W}$

$\gamma = \frac{\partial w}{\partial r}$

Substitution of equation (2b) into equation (1) yields the governing linear partial differential equation

$$\frac{\partial^2 V}{\partial r^2} + \frac{1}{r}\frac{\partial V}{\partial r} - \frac{1}{\nu}\frac{\partial V}{\partial t} = \frac{1}{r}\frac{k}{\mu} \tag{3}$$

where

$\nu = \frac{\mu}{\rho}$ coefficient of kinematic viscosity

The initial conditions are taken to be

$$V = 0 \qquad (t = 0, \quad r > a) \tag{4}$$

$$V = V_o \qquad (t = 0, \quad r \leqq a) \tag{5}$$

where V_o is the initial velocity of the combined mass of the projectile and plug of target material of radius a. In this study V_o is determined from the conservation of momentum at the instant of impact in which the projectile-plug combination is assumed to be rigid and to act as a unit. Thus

$$V_o = g_o \frac{M_1}{M} \tag{6}$$

where

g_o initial velocity of free projectile

M_1 mass of projectile

$M = M_1 + \pi a^2 h\rho$ combined mass of projectile and plug

The boundary conditions are as follows: at $t > 0$, $r = a$

from Newton's second law

$$-\zeta k + \mu\zeta \frac{\partial V}{\partial r} - \frac{\partial V}{\partial t} = 0 \tag{7}$$

where

$$\zeta = \frac{2\pi ah}{M}$$

and at $t \geqq 0$, $r \to \infty$

$$V \to 0 \tag{8}$$

Method of Solution

An analytical solution to the governing equations is obtained in reference 1 by Laplace transform techniques in a manner similar to the approach used in reference 5. The homogeneous solution can be written directly in terms of modified Bessel functions. The particular solution, however, is obtained by utilizing Struve functions of order zero rather than by the method of variation of parameters used in reference 5. The solution to the governing differential equation, equation (3), and its associated boundary conditions (eqs. (4), (5), (7), and (8)) is discussed in detail in the appendix. The solutions obtained are "short time" solutions in t corresponding to values of the transform parameter $s \gg \frac{\nu}{a^2}$ or $t \ll \frac{a^2}{4\nu}$ (see appendix) resulting from the use of asymptotic expansions in the transformed state. It is shown in the appendix that the velocity (A34), displacement (A37), shear strain (A36), and shear strain rate (A35) can be expressed in dimensionless form in terms of a dimensionless radius $\bar{r}$ and a dimensionless time $\bar{t}$.

When the yield strength k is taken to be zero in the equations given in the appendix they reduce to the identical expressions given in reference 3. Also in the case of the

infinite mass projectile in which $H = 0$ $(M_1 = \infty)$ the expression given in equation (A34) for velocity reduced to $V = V_o$ at $\bar{r} = 1$ for all values of $\bar{t} \geqq 0$.

Separation Criterion

In order to determine the radius of the plug of plate material which is sheared (or perforated) from the plate upon impact a separation criterion (identical to that discussed in refs. 1, 2, 3, and 5) consisting of two conditions is established. The first condition for separation is based on the assumption that detachment of the projectile and a portion of the plate material occurs when the plate material can no longer transmit a given shear stress. If the plate behaves in a highly viscous manner it is capable of transmitting a shear stress of any magnitude. In this analysis it is assumed that the material is highly viscous when the strain rate is above some limiting value, here assumed to be k/μ. Below this value only a limited shear stress can be transmitted and consequently separation may take place. This condition of high shear stress and visco-plastic flow will exist immediately after impact when the strain rate is at a maximum and the viscous stress $\mu \frac{\partial \dot{w}}{\partial r}$ is much greater than the yield strength k of the material (see eq. (2b)). In equation form the strain-rate criterion for separation is

$$\left|\left(\frac{\partial \dot{w}}{\partial r}\right)\right|_{cr} = \frac{k}{\mu} \tag{9}$$

The second condition deals with the shear strain of the material which, at the moment of impact, is zero and increases thereafter. In order for the plug to separate from the plate the material not only has to be considered as having a sufficiently small strain rate but must experience large shear strains as well. In this analysis the shear strains are considered large when the shear strain exceeds the dynamic value of the ultimate shear strain of the material.

Thus the second condition can be written as

$$\gamma_{cr} = \left|\left(\frac{\partial w}{\partial r}\right)\right|_{cr} = C_1 \tag{10}$$

where C_1 = dynamic ultimate strain in shear (a value of $C_1 = 0.02$ was used in this paper for both aluminum and steel). For a further discussion of these separation conditions, see references 1, 2, and 3.

The radius of separation of the plug material and the time of separation can most readily be determined by a graphical procedure. In figure 2 a typical nondimensional set of strain distributions for different values of the time parameter $\bar{t}$ is shown. In figure 3 nondimensional strain-rate distributions are shown for a projectile of mass 0.052 g and initial velocity 1.2 km/s impacting on a 0.635-cm (1/4-in.) aluminum plate. A plot of the locus of critical strain points in a $\bar{r},\bar{t}$ space can now be obtained from figure 2 by constructing a horizontal line representing the critical strain (eq. (10)) and determining its $\bar{r},\bar{t}$ intercepts with the strain curves.

In a similar manner the critical strain-rate locus in $\bar{r},\bar{t}$ space can be determined from figure 3. The radius of perforation and the time of separation are now determined from the intersection of the critical strain and critical strain-rate curves as plotted in figure 4. Thus for this particular case the radius of perforation and the time of separation as found from figure 4 are $\bar{r}_p = 1.740$ and $\bar{t} = 0.250$, respectively.

Note that four regions are indicated in figure 4. In these regions the predominant material behavior could be described as follows: large strain rates, large strain (region I); large strain rates, small strain (region II); small strain rate, small strain (region III); small strain rate, large strain (region IV). Only in region IV are both critical conditions of the separation criterion satisfied, and since separation will occur at the first time at which both conditions are satisfied it is assumed that at the apex of this region separation occurs. After initial separation the solution is no longer valid due to the changes in the boundary conditions.

EFFECTS OF PERTINENT PARAMETERS ON PERFORATION RADIUS

Expressions are derived in the appendix for the velocity, displacement, shear strain, and shear strain rate written in nondimensional form. These expressions contain pertinent parameters associated with the perforation problem such as projectile mass, radius, and initial velocity, and target

density, viscosity, yield strength, and thickness. Variations in these pertinent parameters are now investigated to determine their effects on the perforation radius. Numerical results are obtained by use of a high-speed digital computer.

Perforation Radius as a Function of Initial Projectile Velocity

In figure 5 is shown the variation in perforation radius versus initial projectile velocity for a 0.635-cm (1/4-in.) aluminum plate and a 0.224-cm (0.088-in.) steel plate being impacted by a 0.119-cm (3/64-in.) radius rigid cylindrical projectile. The mass of the projectile was taken to be 0.052 g which for aluminum corresponds to a projectile 0.434 cm (0.171 in.) long. Note that the mass per unit area of the steel plate is equivalent to the mass per unit area of the aluminum plate. Thus the momentum exchange between the impacting projectile and both the steel and aluminum plates is identical.

As can be seen from figure 5, the inclusion of material yield strength in the analysis has little effect on the perforation radius for the range of velocities shown (maximum difference is of the order of 5 percent). Although steel has a higher yield strength than aluminum, the critical strain rate, which depends on viscosity as well as yield strength, is for steel, only 2/3 of that for aluminum $\left(\mu = 15\ \frac{kNs}{m^2}\right.$ (0.15 megapoise), $k = 1.38\ \frac{GN}{m^2}$ (200 ksi) for steel; $\mu = 5\ \frac{kNs}{m^2}$ (0.05 megapoise), $\left.k = 0.69\ \frac{GN}{m^2}\right.$ (100 ksi) for Al). Hence, for the same

initial velocity, the perforation radius in steel is larger than in aluminum and separation occurs in the steel plate after a greater passage of time.

Perforation Radius as a Function of Projectile Mass or Plate Thickness

The effect of varying the thickness of the aluminum plate on the nondimensional perforation radius is shown in figure 6. The initial velocity of the aluminum projectile was taken to be 6.1 km/s and the plate thickness was varied from 0.635 cm to 6.35 cm (1/4 in. to 2.5 in.) all other parameters being held constant. The increase in plate thickness decreases the perforation radius and time of separation. The inclusion of yield strength in the analysis has little effect on the calculated perforation radii (maximum variation in calculated radii is of the order of 4 percent). Note in addition if the mass of the projectile is decreased by a factor (the radius remaining constant) instead of the plate thickness being increased by the same factor, the calculated results are identical. This result is due to the fact that the nondimensional parameter H,

$$H = \frac{2}{1 + \frac{1}{\pi a^2 \rho}\left(\frac{M_1}{h}\right)} \tag{11}$$

changes in the same proportion with decrease in M_1 or increase in h. The perforation radii are thus seen to decrease with either a decrease in projectile mass or an increase in plate thickness. It is evident from figure 6

that the effects of yield strength need not be considered in the calculation of perforation radii.

Perforation Radius as a Function of Coefficient of Dynamic Viscosity

The variation in nondimensional perforation radii due to changes in the coefficient of dynamic viscosity is shown in figure 7, for the 0.052-g projectile impacting on the aluminum plate. A velocity of 1.2 km/s was chosen and the coefficient of dynamic viscosity was varied from 0 to 15 $\frac{kNs}{m^2}$ (0.15 megapoise), all the other parameters remained constant and are given in figure 7. Although calculations were made for larger values of μ, it was found that the dimensionless separation times exceeded the limits of the applicability of the short time solution.

Note that as the coefficient of dynamic viscosity is increased, the resulting perforation radii also increase. A small variation in the coefficient of viscosity is shown to produce a large variation in perforation radii, and indicates a definite need for better evaluation of this coefficient. The inclusion of the yield strength in the analysis results in perforation radii as much as 10 percent lower than the solution with yield strength taken to be zero. However, this variation can be considered to be negligible in comparison to the variation caused by changes in viscosity.

Perforation Radius as a Function of Projectile Radius

The effect of varying the projectile dimensions on the perforation radius (in units) is shown in figure 8. The mass and impacting velocity of the projectile were considered to remain constant at 0.052 g and 6.1 km/s, respectively. The target plate was considered to be made of aluminum of 0.635-cm (1/4-in.) thickness. The figure illustrates that as the shape of the cylindrical projectile changes from that of a pencil to that of a disk (note projectile schematics in fig. 8) the perforation radius increases. It is important to recognize that the ratio of perforation radius to projectile radius is diminishing with increasing projectile radius. The effect of including dynamic yield strength in computing perforation radii is seen to be negligible in comparison to the effects produced by varying the projectile radius.

Perforation Radius as a Function of Dynamic Yield Strength for a Fixed Separation Criterion

The calculations presented earlier for the aluminum target plate have assumed a value of dynamic yield strength in shear of 0.69 $\frac{GN}{m^2}$ (100 ksi). A great deal of uncertainty exists in determining the dynamic yield strength especially under hypervelocity impact conditions. To determine the effects of wide variations in strength on the computed perforation radii the dynamic yield strength has been varied from 0 to 6.9 $\frac{GN}{m^2}$ (1,000 ksi) and the calculated perforation radii are shown plotted in figure 9. These perforation radii are

determined using a constant value of the critical strain rate $\left(\left|\left(\frac{\partial V}{\partial r}\right)_{cr} \frac{a}{V_o}\right| = 0.0692\right)$. If the critical strain rate, (k/μ), has also been varied in accord with the variation in dynamic yield strength k, keeping μ constant, then as the yield strength approaches zero the critical strain rate would also approach zero and the perforation radius would approach infinity. This result is unrealistic and the critical strain rate therefore is not varied according to the variation in k but is assumed to remain constant.

Figure 9 again illustrates that the effect of including dynamic yield strength in the calculation of perforation radii is negligible for reasonable values of dynamic yield strength. As can be seen from the figure, the decrease in perforation radii for an increase of the dynamic yield strength between 0 and 3.45 $\frac{GN}{m^2}$ (500 ksi) is less than 10 percent.

Comments on the Effects of Yield Strength on Velocities, Displacements, and Stresses

In the previous sections, it has been shown that the results for perforation radii obtained with the inclusion of yield strength in the analysis differ little from the results in which yield strength was taken to be zero. In reference 1 many calculations have been made on velocities, displacements, and stresses with and without yield strength considerations and a few pertinent remarks on these results are in order. The strain and strain rates are little affected by the inclusion of yield strength terms and result in similar curves

when plotted as a function of plate radii. The velocities, displacements, and stresses of the solution containing yield strength, however, are at times markedly different from the solution in which yield strength is taken to be zero. The effects of yield strength in general are to produce much smaller velocities and much smaller displacements than when the yield strength is taken to be zero. In fact, for the particular case where the projectiles do not perforate the target plate, the analysis including yield strength indicates the velocity drops to zero and the plate becomes rigid in a deformed state, while if the yield strength is taken to be zero the velocity approaches a nonzero limiting value, and the plate continues to deform. A more complete discussion and analysis of the effects of target material yield strength on the velocities, displacements, and stresses of the target plate is given in reference 1.

BALLISTIC LIMITS OF THIN PLATES

Another question of prime concern in the investigation of hypervelocity impact is that of establishing minimum thickness requirements of thin plates necessary for the prevention of projectile perforation. This minimum plate thickness or maximum projectile velocity allowable before perforation initiates is termed the ballistic limit. The ballistic limit was determined in the following manner. The graphical procedure as illustrated in figure 4 by the intersection of the critical

strain and critical strain-rate curves, establishes the radius and time of separation of the plug of plate material being sheared from the target plate. By decreasing the initial projectile velocity, the critical strain curve in figure 4 rises, and the critical strain-rate curve decreases and bends more sharply toward the ordinate $\bar{t}$. Thus, the radius of perforation and time of separation decrease until the intersection of the two curves occurs at $\bar{r} = 1$. For any further decrease in initial projectile velocity, the curves will not intersect and a ballistic limit is assumed to have been reached. Note that under the assumptions adopted in this paper no considerations have been made for spallation. The ballistic limits established in this manner for thin target plates could yield plate thicknesses which are unconservative (i.e., too thin to prevent perforation for a given projectile velocity) and comparison with experimental data is essential to ascertain the degree of error introduced in neglecting the effect of spallation of the target plate.

The ballistic limit thickness as a function of projectile mass for six different projectile velocities is shown in figure 10. The projectile velocities were varied from 0.914 km/s to 6.462 km/s. However, the projectile radius was held constant at 0.32 cm (1/8 in.). The curves which are shown in the figure are valid for $k = 0.69 \frac{GN}{m^2}$ (100 ksi) and the projectile velocity shown above the curves, and for $k = 0$ and the projectile velocity shown below the curves. The inclusion of

the material yield strength in ballistic limit studies produces effects which are only slightly higher (approximately 10 percent) than those presented earlier on perforation studies (approximately 5 percent).

The minimum plate thicknesses are shown plotted as a function of initial projectile velocity for three different mass projectiles in figure 11. Figure 11 is simply a cross plot of figure 10, considering the mass M_1 constant. The radius of the projectile is held constant at 0.32 cm (1/8 in.), but the mass is varied from 0.001 g to 0.100 g. This change in mass could be accomplished by either changing the length or the density of the projectile. Note that the curves are all parallel and increase as $(g_o)^{1.05}$. This velocity dependence is quite similar to experimental results obtained for the dependence of penetration on the velocity of the impacting projectile by Collins and Kinard (ref. 8).

In figure 12 the minimum plate thickness is again plotted as a function of projectile mass for eight different projectile velocities. The radius of the projectile, however, has now been decreased to 0.119 cm (3/64 in.). Notice how sharply the minimum plate thicknesses have increased from figure 10 to figure 12. In the case of a projectile of mass 0.01 g, the minimum plate thickness differs by a factor of five and a half considering the projectile first to have a radius of 0.32 cm (1/8 in.) and then a radius of 0.119 cm (3/64 in.). Under these conditions, the same density

material would resemble first a disklike projectile and then a bulletlike projectile as the radius is decreased. Hence, projectile aspect ratio is most important in determining the ballistic limit of thin plates, exhibiting a much more influential effect on the results than is evident in perforation studies.

CONCLUDING REMARKS

It is shown that the inclusion of target material yield strength in a one-dimensional analysis of hypervelocity impact perforations produces little effect on the resulting perforation radius. The variation in calculated perforation radius as compared to the solution with target yield strength taken to be zero generally amounted to only 5 percent in this investigation. This difference in calculated perforation radii remains at the negligible 5-percent level even with variations in the pertinent parameters such as plate (or target) thickness, projectile mass, and initial velocity. With variations in the coefficient of dynamic viscosity, however, the difference due to yield strength does increase to perhaps 10 percent. On the other hand, the variation in perforation radius due to differences in the assumed value of the viscosity coefficient alone can be much greater than the 10 percent. Consequently, the determination of accurate values for the coefficient of dynamic viscosity is much more critical to the calculation

of perforation radius than is the inclusion of the target yield strength.

In the determination of the ballistic limits of thin plates (that minimum allowable thickness or maximum allowable velocity) the effect of including yield strength in the analysis produces results which differ by approximately 10 percent from the analysis with yield strength taken to be zero. A much more critical parameter was found to be the radius of the impacting projectile. The aspect ratio of the impacting projectile (in this case a right circular cylinder), in changing from a disklike projectile to a pencillike projectile of the same mass, produces ballistic limits which differ considerably. Obviously the radius of the impacting projectile is therefore a factor of prime importance, and the yield strength of the plate material one of secondary importance in ballistic limit studies. It was noted that the nearly linear velocity dependence in the determination of ballistic limits was quite similar to experimental results obtained in the penetration studies of reference 8.

APPENDIX

GOVERNING EQUATION OF SHEAR PERFORATION

In this appendix an analytical solution is presented for the governing linear differential equation and its associated boundary conditions. In a manner similar to that employed by Chou in reference 3, the governing partial differential equation is reduced to a total differential equation by use of Laplace transform techniques. To obtain a particular solution to the resulting total differential equation a further change in variables becomes necessary. After satisfying the associated boundary conditions a "short time" solution is determined by employing asymptotic approximations in the transformed state.

The governing linear differential equation of motion in the axial direction, for simple shear perforation, as derived in the text (see eq. (3)) can be written as

$$\frac{\partial^2 V}{\partial r^2} + \frac{1}{r}\frac{\partial V}{\partial r} - \frac{1}{\nu}\frac{\partial V}{\partial t} = \frac{1}{r}\frac{k}{\mu} \qquad \text{(A1)}$$

transforming equation (A1) with respect to t by use of Laplace transform techniques, results in

$$\frac{d^2\overline{V}}{dr^2} + \frac{1}{r}\frac{d\overline{V}}{dr} - \frac{1}{\nu}\left[s\overline{V} - V(o,r)\right] = \frac{1}{r}\frac{k}{\mu s} \qquad \text{(A2)}$$

where s is the transform parameter. By use of the initial condition (eq. (4)), $V(o,r) = 0$ at $t = 0$, $r > a$ equation (A2) is reduced to

$$\frac{d^2\bar{V}}{dr^2} + \frac{1}{r}\frac{d\bar{V}}{dr} - \frac{s\bar{V}}{\nu} = \frac{1}{r}\frac{k}{\mu s} \tag{A3}$$

Let

$$r = \frac{-iz}{\sqrt{\frac{s}{\nu}}} \tag{A4}$$

hence

$$\frac{d\bar{V}}{dr} = \frac{d\bar{V}}{dz}\, i\sqrt{\frac{s}{\nu}} \tag{A5}$$

$$\frac{d^2\bar{V}}{dr^2} = \frac{-d^2\bar{V}}{dz^2}\frac{s}{\nu} \tag{A6}$$

and by substitution of the above relations into equation (A3) there results

$$\frac{d^2\bar{V}}{dz^2} + \frac{1}{z}\frac{d\bar{V}}{dz} + \bar{V} = \frac{-i}{\sqrt{\frac{s}{\nu}}}\frac{k}{\mu s z} \tag{A7}$$

The homogeneous solution can be written directly as

$$\bar{V}_H(z) = AJ_o(z) + BY_o(z) \tag{A8}$$

For the particular solution to equation (A7) the Struve function of zero order is satisfactory. A known relation for the Struve function of order p is (see ref. 9, p. 211)

$$\frac{d^2S_p(z)}{dz^2} + \frac{1}{z}\frac{dS_p(z)}{dz} + \left(1 - \frac{p^2}{z^2}\right)S_p(z) = \frac{\left(\frac{z}{2}\right)^{p-1}}{\sqrt{\pi}(p - 0.5)!} \tag{A9}$$

Let $p = 0$

$$\frac{d^2S_o(z)}{dz^2} + \frac{1}{z}\frac{dS_o(z)}{dz} + S_o(z) = \frac{2}{z\pi} \tag{A10}$$

Hence, the particular solution to equation (A7) can be written as

$$\bar{V}_p(z) = -\frac{\pi i}{2\sqrt{\frac{s}{\nu}}}\frac{k}{\mu s}S_o(z) \tag{A11}$$

and the general solution becomes

$$\bar{V}(z) = \bar{V}_H(z) + \bar{V}_p(z) = AJ_o(z) + BY_o(z) - \frac{\pi i k}{2\sqrt{\frac{s}{\nu}}\mu s}S_o(z) \tag{A12}$$

or, resubstituting for z from equation (A4)

$$\bar{V}(r,s) = AJ_o\left(ir\sqrt{\frac{s}{\nu}}\right) + BY_o\left(ir\sqrt{\frac{s}{\nu}}\right) - \frac{\pi i k}{2\sqrt{\frac{s}{\nu}}\mu s}S_o\left(ir\sqrt{\frac{s}{\nu}}\right) \tag{A13}$$

In order to apply now the (transformed) boundary condition given by equation (8), namely, $\bar{V} = 0$ as $r \to \infty$ one must consider the asymptotic behavior of the solution as given by equation (A13) for $|r| \gg 1$. The asymptotic approximation for the Struve function of order zero as found in reference 9, equation (136a) is

$$S_o\left(ir\sqrt{\frac{s}{\nu}}\right) \approx Y_o\left(ir\sqrt{\frac{s}{\nu}}\right) + \frac{2}{\pi i r\sqrt{\frac{s}{\nu}}} \tag{A14}$$

and since a known identity between the Bessel functions is (see ref. 10, eq. (110))

$$K_o\left(r\sqrt{\frac{s}{\nu}}\right) = \frac{\pi}{2}i\left[I_o\left(r\sqrt{\frac{s}{\nu}}\right) + iY_o\left(ir\sqrt{\frac{s}{\nu}}\right)\right] \tag{A15}$$

then

$$S_o\left(ir\sqrt{\frac{s}{\nu}}\right) \approx iI_o\left(r\sqrt{\frac{s}{\nu}}\right) - \frac{2}{\pi}K_o\left(r\sqrt{\frac{s}{\nu}}\right) + \frac{2}{\pi i r\sqrt{\frac{s}{\nu}}} \tag{A16}$$

Hence, for $|r| \gg 1$, the general solution can be written as

$$\bar{V}(r,s) \approx AI_o\left(r\sqrt{\frac{s}{\nu}}\right) + B\left[iI_o\left(r\sqrt{\frac{s}{\nu}}\right) - \frac{2}{\pi}K_o\left(r\sqrt{\frac{s}{\nu}}\right)\right]$$
$$+ \frac{\pi k}{2\sqrt{\frac{s}{\nu}}\mu s}I_o\left(r\sqrt{\frac{s}{\nu}}\right) + \frac{ik}{\sqrt{\frac{s}{\nu}}\mu s}K_o\left(r\sqrt{\frac{s}{\nu}}\right) - \frac{k}{r\frac{s^2}{\nu}\mu} \qquad (A17)$$

Application of the transformed boundary condition, $\bar{V} = 0$ as $r \to \infty$ (see eq. (8)) yields the relation

$$A = -B_i - \frac{\pi k}{2\sqrt{\frac{s}{\nu}}\mu s} \qquad (A18)$$

Since $K_o \to 0$ and $I_o \to \infty$ as $r \to \infty$. Use of the known identities between $K_o\left(r\sqrt{\frac{s}{\nu}}\right)$ (eq. (A15)), $S_o\left(ir\sqrt{\frac{s}{\nu}}\right)$ (eq. (A14)), $I_o\left(r\sqrt{\frac{s}{\nu}}\right)$, and $Y_o\left(ir\sqrt{\frac{s}{\nu}}\right)$ reduces the general solution to

$$\bar{V}(r,s) = -B\frac{2}{\pi}K_o\left(r\sqrt{\frac{s}{\nu}}\right) - \frac{\pi k}{2\sqrt{\frac{s}{\nu}}\mu s}I_o\left(r\sqrt{\frac{s}{\nu}}\right) - \frac{\pi ik}{2\sqrt{\frac{s}{\nu}}\mu s}S_o\left(ir\sqrt{\frac{s}{\nu}}\right) \qquad (A19)$$

The quantity B is now evaluated by application of the (transformed) boundary condition (see eq. (7); note also eq. (5)):

$$S\bar{V} - \zeta\mu\frac{d\bar{V}}{dr} + \zeta\frac{k}{s} = V_o \qquad (r = a,\ t > 0) \qquad (A20)$$

Substitution of equation (A19) into equation (A20) and by use of equation (140a) of reference 10 yields the following expression for B:

$$B = -V_o - \frac{\pi k}{2\sqrt{\frac{s}{\nu}}\mu}I_o\left(a\sqrt{\frac{s}{\nu}}\right) - S_o\left(ia\sqrt{\frac{s}{\nu}}\right)\frac{\pi ik}{2\mu\sqrt{\frac{s}{\nu}}}$$
$$+ \zeta\frac{\pi k}{2s}I_1\left(a\sqrt{\frac{s}{\nu}}\right) - \zeta\frac{\pi k}{2s}\left[\frac{2}{\pi} - S_1\left(ia\sqrt{\frac{s}{\nu}}\right)\right] \qquad (A21)$$
$$+ \zeta\frac{k}{s} \div \frac{2}{\pi}\left(sK_o\left(a\sqrt{\frac{s}{\nu}}\right) + \zeta\mu\sqrt{\frac{s}{\nu}}K_1\left(a\sqrt{\frac{s}{\nu}}\right)\right)$$

Hence, the general solution can be written as

$$\bar{V}(r,s) = \left[V_o + \frac{\pi k}{2\sqrt{\frac{s}{\nu}}\mu} I_o\left(a\sqrt{\frac{s}{\nu}}\right) + S_o\left(ia\sqrt{\frac{s}{\nu}}\right)\frac{\pi i k}{2\mu\sqrt{\frac{s}{\nu}}} - \zeta\frac{\pi k}{2s} I_1\left(a\sqrt{\frac{s}{\nu}}\right) \right.$$

$$\left. + \zeta\frac{\pi k}{2s}\left[\frac{2}{\pi} - S_1\left(ia\sqrt{\frac{s}{\nu}}\right)\right] - \zeta\frac{k}{s}\right] K_o\left(r\sqrt{\frac{s}{\nu}}\right) \div \left[sK_o\left(a\sqrt{\frac{s}{\nu}}\right) \right.$$

$$\left. + \zeta\mu\sqrt{\frac{s}{\nu}} K_1\left(a\sqrt{\frac{s}{\nu}}\right)\right] - \frac{\pi k}{2\mu s\sqrt{\frac{s}{\nu}}} I_o\left(r\sqrt{\frac{s}{\nu}}\right) - S_o\left(ir\sqrt{\frac{s}{\nu}}\right)\frac{\pi i k}{2\mu s\sqrt{\frac{s}{\nu}}} \quad \text{(A22)}$$

A "short time" solution is now determined from the general solution by assuming $a\sqrt{\frac{s}{\nu}} > 1$. By reference again to equation (136a) of reference 10, it can be shown that

$$S_1\left(ia\sqrt{\frac{s}{\nu}}\right) \approx Y_1\left(ia\sqrt{\frac{s}{\nu}}\right) + \frac{2}{\pi} - \frac{2}{\pi a^2\frac{s}{\nu}} \quad \text{(A23)}$$

A known identity between the modified Bessel function of the second kind of order one K_1 and the Hankel function of the first kind of order one $H_1^{(1)}$ is (see ref. 10, eqs. (115) and (70))

$$K_1\left(a\sqrt{\frac{s}{\nu}}\right) = -\frac{\pi}{2}H_1^{(1)}\left(ia\sqrt{\frac{s}{\nu}}\right) = -\frac{\pi}{2}\left[J_1\left(ia\sqrt{\frac{s}{\nu}}\right) + iY_1\left(ia\sqrt{\frac{s}{\nu}}\right)\right] \quad \text{(A24)}$$

Hence

$$J_1\left(ia\sqrt{\frac{s}{\nu}}\right) = -iY_1\left(ia\sqrt{\frac{s}{\nu}}\right) - \frac{2}{\pi}K_1\left(a\sqrt{\frac{s}{\nu}}\right) \quad \text{(A25)}$$

and since

$$I_1\left(a\sqrt{\frac{s}{\nu}}\right) = -iJ_1\left(ia\sqrt{\frac{s}{\nu}}\right) \quad \text{(A26)}$$

then, from equation (A25)

$$I_1\left(a\sqrt{\frac{s}{\nu}}\right) = -Y_1\left(ia\sqrt{\frac{s}{\nu}}\right) + \frac{2i}{\pi}K_1\left(a\sqrt{\frac{s}{\nu}}\right) \tag{A27}$$

Thus

$$\frac{2}{\pi} - S_1\left(ia\sqrt{\frac{s}{\nu}}\right) \approx I_1\left(a\sqrt{\frac{s}{\nu}}\right) + \frac{2}{\pi a^2\frac{s}{\nu}} - \frac{2i}{\pi}K_1\left(a\sqrt{\frac{s}{\nu}}\right) \tag{A28}$$

Substitution of the asymptotic expressions for S_o and $\frac{2}{\pi} - S_1$ into the general solution (eq. (A22)) and making use of the identity for Y_o (eq. (A15)) yields

$$\overline{V}(r,s) = \frac{\left(V_o + \frac{k}{a\rho s} - \zeta\frac{k}{s} + \zeta\frac{k\nu}{a^2s^2}\right)K_o\left(r\sqrt{\frac{s}{\nu}}\right)}{sK_o\left(a\sqrt{\frac{s}{\nu}}\right) + \zeta\mu\sqrt{\frac{s}{\nu}}K_1\left(a\sqrt{\frac{s}{\nu}}\right)} - \frac{k}{\rho s^2 r} \tag{A29}$$

Note that for increased accuracy in equation (A29), it is only necessary to increase the number of terms taken in the asymptotic expansions of S_o and S_1; of course, the semiconvergent nature of the asymptotic expansions must be considered. These additional terms are polynomials and would not present any new difficulties. To aid in determining the inverse transform of equation (A29), the following asymptotic expansions of the modified Bessel functions K_0, K_1 are employed (see eq. (114) of ref. 10)

$$\left.\begin{aligned} K_0(z) &= \sqrt{\frac{\pi}{2z}}e^{-z}\left(1 - \frac{1}{8z} + \frac{9}{128z^2} + \cdots\right) \\ K_1(z) &= \sqrt{\frac{\pi}{2z}}e^{-z}\left(1 + \frac{3}{8z} - \frac{15}{128z^2} + \cdots\right) \end{aligned}\right\} \tag{A30}$$

Substitution of the asymptotic expansions given in equation (A30) into equation (A29) yields, after algebraic manipulation

$$\bar{V}(r,s) = \left(\frac{a}{r}\right)^{\frac{1}{2}} e^{-\sqrt{\frac{s}{\nu}}(r-a)}\left[\frac{V_o}{s} + \frac{1}{s^2}\left(\frac{k}{a\rho} - \zeta k\right) + \frac{1}{s^3}\zeta\frac{k\nu}{a^2}\right]\left[1 - \left(\zeta\frac{\mu}{\nu} + \frac{a-r}{8ra}\right)\frac{1}{\sqrt{\frac{s}{\nu}}}\right.$$

$$\left. + \left(\frac{9a^2 - 2ar - 7r^2}{128a^2r^2} + \zeta\frac{\mu}{\nu}\frac{a-5r}{8ra} + \zeta^2\frac{\mu^2}{\nu^2}\right)\frac{1}{s/\nu} + \cdots\right] - \frac{k}{\rho s^2 r} \quad \text{(A31)}$$

and by application of standard transform tables (ref. 11, p. 380, formulas (11)) $\bar{V}$ becomes

$$V(r,t) = V_o\left(\frac{a}{r}\right)^{1/2}\left[\operatorname{erfc}\frac{r-a}{2\sqrt{\nu t}} + \left(\frac{r-a}{8r} - \zeta\frac{\mu a}{\nu}\right)\frac{2\sqrt{\nu t}}{a}\,i\operatorname{erfc}\frac{r-a}{2\sqrt{\nu t}}\right.$$

$$\left. + \left(\frac{9a^2 - 2ar - 7r^2}{128r^2} + \zeta\frac{\mu a}{\nu}\frac{a-5r}{8r} + \zeta^2\frac{\mu^2a^2}{\nu^2}\right)\frac{4\nu t}{a^2}i^2\operatorname{erfc}\frac{r-a}{2\sqrt{\nu t}} \cdots\right]$$

$$+ k\left(\frac{1}{\rho a} - \zeta\right)\left(\frac{a}{r}\right)^{1/2}\left[4ti^2\operatorname{erfc}\frac{r-a}{2\sqrt{\nu t}} + \left(\frac{r-a}{8r} - \zeta\frac{\mu a}{\nu}\right)\frac{\sqrt{\nu}}{a}(4t)^{3/2}i^3\operatorname{erfc}\frac{r-a}{2\sqrt{\nu t}}\right.$$

$$\left. + \left(\frac{9a^2 - 2ar - 7r^2}{128r^2} + \zeta\frac{\mu a}{\nu}\frac{a-5r}{8r} + \zeta^2\frac{\mu^2a^2}{\nu^2}\right)\frac{16\nu t^2}{a^2}i^4\operatorname{erfc}\frac{r-a}{2\sqrt{\nu t}} \cdots\right]$$

$$+ \zeta\frac{k\mu}{\rho a^2}\left(\frac{a}{r}\right)^{1/2}\left[16t^2i^4\operatorname{erfc}\frac{r-a}{2\sqrt{\nu t}} + \left(\frac{r-a}{8r} - \zeta\frac{\mu a}{\nu}\right)\frac{\sqrt{\nu}}{a}(4t)^{5/2}i^5\operatorname{erfc}\frac{r-a}{2\sqrt{\nu t}}\right.$$

$$\left. + \left(\frac{9a^2 - 2ar - 7r^2}{128r^2} + \zeta\frac{\mu a}{\nu}\frac{a-5r}{8r} + \zeta^2\frac{\mu^2a^2}{\nu^2}\right)\frac{\nu}{a^2}64t^3i^6\operatorname{erfc}\frac{r-a}{2\sqrt{\nu t}} \cdots\right] - \frac{kt}{\rho r}$$

$$\left((r-a) \geqq 0\right) \quad \text{(A32)}$$

where the symbol i^n denotes the nth integral of the complementary error function.

Equation (A32) can now be nondimensionalized as follows:

Let

$$\left.\begin{aligned} \bar{r} &= \frac{r}{a} \\ \bar{t} &= \frac{\nu t}{a^2} \\ H &= \zeta\frac{\mu a}{\nu} = \frac{2\pi a^2 h\rho}{M} \\ K &= \frac{ka}{V_o\mu} \end{aligned}\right\} \tag{A33}$$

Hence, the nondimensional velocity can be written as

$$\begin{aligned} \frac{V}{V_o} = \frac{1}{\sqrt{\bar{r}}}\Bigg\{ & \operatorname{erfc}\frac{\bar{r}-1}{2\sqrt{\bar{t}}} + 4K(1-H)\bar{t}i^2\operatorname{erfc}\frac{\bar{r}-1}{2\sqrt{\bar{t}}} + 16KH\bar{t}^2i^4\operatorname{erfc}\frac{\bar{r}-1}{2\sqrt{\bar{t}}} \\ & + R_1\left[2\sqrt{\bar{t}}i\ \operatorname{erfc}\frac{\bar{r}-1}{2\sqrt{\bar{t}}} + 8K(1-H)\bar{t}i^3\operatorname{erfc}\frac{\bar{r}-1}{2\sqrt{\bar{t}}} + 32KH(\bar{t})^{5/2}i^5\operatorname{erfc}\frac{\bar{r}-1}{2\sqrt{\bar{t}}}\right] \\ & + R_2\left[4\bar{t}i^2\operatorname{erfc}\frac{\bar{r}-1}{2\sqrt{\bar{t}}} + 16K(1-H)\bar{t}^2i^4\operatorname{erfc}\frac{\bar{r}-1}{2\sqrt{\bar{t}}} + 64KH\bar{t}^3\operatorname{erfc}\frac{\bar{r}-1}{2\sqrt{\bar{t}}}\right]\cdots\Bigg\} - \frac{K\bar{t}}{\bar{r}} \end{aligned} \tag{A34}$$

$$\left((\bar{r}-1)\geq 0\right)$$

where

$$R_1 = \frac{1}{8} - \frac{1}{8\bar{r}} - H$$

$$R_2 = \frac{1}{128\bar{r}^2} - \frac{1}{64\bar{r}} - \frac{7}{128} + H\left(\frac{1}{8\bar{r}} - \frac{5}{8}\right) + H^2$$

By comparison of equations (A31) and (A32), it can be shown that s is related to $1/4t$ and that $a\sqrt{s/\nu} > 1$ implies $\bar{t} < 1/4$. Nevertheless, calculations indicate that the three-term asymptotic series presented in equation (A30) are only approximately 10 to 15 percent in error for $\bar{t} = 1/2$ (and

$a\sqrt{s/\nu} = 1/\sqrt{2}\Big)$. Therefore, results are presented in this paper for values of $\bar{t}$ as high as 1/2. Results for $\bar{t} > 1/2$ should be viewed with increasing skepticism. Differentiation of equation (A38) with respect to $\bar{r}$ yields the nondimensional shear strain rate

$$\frac{\partial V}{\partial r}\frac{a}{V_o} = \frac{1}{\sqrt{\bar{r}}}\left\{-\frac{1}{\sqrt{\pi\bar{t}}}e^{-\frac{(\bar{r}-1)^2}{4\bar{t}}} + R_3\,\mathrm{erfc}\,\frac{\bar{r}-1}{2\sqrt{\bar{t}}} + 2\sqrt{\bar{t}}\left[R_4 - K(1-H)\right]i\,\mathrm{erfc}\,\frac{\bar{r}-1}{2\sqrt{\bar{t}}}\right.$$

$$+ 4\bar{t}\left[R_5 + K(1-H)R_3\right]i^2\mathrm{erfc}\,\frac{\bar{r}-1}{2\sqrt{\bar{t}}} + 8(\bar{t})^{3/2}\left[K(1-H)R_4 - KH\right]i^3\,\mathrm{erfc}\,\frac{\bar{r}-1}{2\sqrt{\bar{t}}}$$

$$+ 16\bar{t}^2\left[KHR_3 + K(1-H)R_5\right]i^4\mathrm{erfc}\,\frac{\bar{r}-1}{2\sqrt{\bar{t}}} + 32(\bar{t})^{5/2}KHR_4i^5\mathrm{erfc}\,\frac{\bar{r}-1}{2\sqrt{\bar{t}}}$$

$$\left. + 64\bar{t}^3KHR_5i^6\,\mathrm{erfc}\,\frac{\bar{r}-1}{2\sqrt{\bar{t}}} \cdots\right\} + \frac{K\bar{t}}{\bar{r}^2} \qquad \left((\bar{r}-1) \geq 0\right) \tag{A35}$$

where

$$R_3 = -\frac{3}{8\bar{r}} - \frac{1}{8} + H$$

$$R_4 = \frac{15}{128\bar{r}^2} - \frac{3}{64\bar{r}} + \frac{7}{128} + \frac{H}{8}\left(\frac{3}{\bar{r}} + 5\right) - H^2$$

$$R_5 = -\frac{45}{256\bar{r}^3} + \frac{3}{128\bar{r}^2} + \frac{7}{256\bar{r}} + \frac{H}{16}\left(\frac{5}{\bar{r}} - \frac{3}{\bar{r}^2}\right) - \frac{H^2}{2\bar{r}}$$

By integration of equation (A35) with respect to $\bar{t}$ the nondimensional shear strain is obtained

$$\frac{\partial w}{\partial r}\frac{\nu}{V_o a} = \frac{4\bar{t}}{\sqrt{\bar{r}}}\left\{-\frac{1}{2\sqrt{\bar{t}}}i\,\mathrm{erfc}\,\frac{\bar{r}-1}{2\sqrt{\bar{t}}} + R_3 i^2\mathrm{erfc}\,\frac{\bar{r}-1}{2\sqrt{\bar{t}}} + 2\sqrt{\bar{t}}\left[R_4 - K(1-H)\right]i^3\mathrm{erfc}\,\frac{\bar{r}-1}{2\sqrt{\bar{t}}}\right.$$

$$+ 4\bar{t}\left[R_5 + K(1-H)R_3\right]i^4\mathrm{erfc}\,\frac{\bar{r}-1}{2\sqrt{\bar{t}}} + 8(\bar{t})^{3/2}\left[K(1-H)R_4 - KH\right]i^5\mathrm{erfc}\,\frac{\bar{r}-1}{2\sqrt{\bar{t}}}$$

$$+ 16\bar{t}^2\left[KHR_3 + K(1-H)R_5\right]i^6\mathrm{erfc}\,\frac{\bar{r}-1}{2\sqrt{\bar{t}}} + 32(\bar{t})^{5/2}KHR_4 i^7\mathrm{erfc}\,\frac{\bar{r}-1}{2\sqrt{\bar{t}}}$$

$$\left. + 64\bar{t}^3 KHR_5 i^8\mathrm{erfc}\,\frac{\bar{r}-1}{2\sqrt{\bar{t}}}\ldots\right\} + \frac{K\bar{t}^2}{2\bar{r}^2} \qquad \left((\bar{r}-1)\geq 0\right) \tag{A36}$$

A second integration with respect to $\bar{r}$ would determine the corresponding displacement. However, a simpler approach is to integrate the nondimensional velocity with respect to $\bar{t}$ to obtain the nondimensional displacement

$$\frac{w}{a^2}\frac{\nu}{V_o} = \frac{4\bar{t}}{\sqrt{\bar{r}}}\left\{i^2\mathrm{erfc}\,\frac{\bar{r}-1}{2\sqrt{\bar{t}}} + 4K(1-H)\bar{t}\,i^4\mathrm{erfc}\,\frac{\bar{r}-1}{2\sqrt{\bar{t}}} + 16\,KH\bar{t}^2 i^6\mathrm{erfc}\,\frac{\bar{r}-1}{2\sqrt{\bar{t}}}\right.$$

$$+ R_1\left[2\sqrt{\bar{t}}\,i^3\mathrm{erfc}\,\frac{\bar{r}-1}{2\sqrt{\bar{t}}} + 8K(1-H)(\bar{t})^{3/2}i^5\mathrm{erfc}\,\frac{\bar{r}-1}{2\sqrt{\bar{t}}} + 32KH(\bar{t})^{5/2}i^7\mathrm{erfc}\,\frac{\bar{r}-1}{2\sqrt{\bar{t}}}\right]$$

$$\left. + R_2\left[4\bar{t}\,i^4\mathrm{erfc}\,\frac{\bar{r}-1}{2\sqrt{\bar{t}}} + 16K(1-H)\bar{t}^2 i^4\mathrm{erfc}\,\frac{\bar{r}-1}{2\sqrt{\bar{t}}} + 64KH\bar{t}^3 i^8\mathrm{erfc}\,\frac{\bar{r}-1}{2\sqrt{\bar{t}}}\right]\ldots\right\} - \frac{K\bar{t}^2}{2\bar{r}}$$

$$\left((\bar{r}-1)\geq 0\right) \tag{A37}$$

The symbol $i^n\mathrm{erfc}\,x$ represents the repeated nth integrals of the complementary error function $\mathrm{erfc}\,\xi$

$$i^n\mathrm{erfc}\,x = \int_x^\infty i^{n-1}\mathrm{erfc}\,\xi\;d\xi \tag{A38}$$

in which

$$i^0\mathrm{erfc}\,x = \mathrm{erfc}\,x$$

$$i^{-1}\mathrm{erfc}\,x = \frac{2}{\sqrt{\pi}}e^{-x^2}$$

A recurrence relation useful in determining the repeated integrals of the complementary error function is (see refs. 10 and 11)

$$i^n\text{erfc } x = \frac{i^{n-2}\text{erfc } x - 2xi^{n-1}\text{erfc } x}{2n} \qquad \text{(A39)}$$

A table of the error function and its derivatives and integrals for values of the argument between 0 and 3.0 is presented in reference 11 from values given in reference 12. A similar table has been included in reference 1 with slight extensions, for convenience of use in computing the above expressions. A table of the first 11 repeated integrals of the error function with values of the argument between 0 and 2.80 is also available in reference 13.

REFERENCES

1. Thomson, Robert G.: Effects of Target Material Yield Strength on Hypervelocity Perforation. NASA TR R- , 1965.

2. Chou, Pei Chi: Perforation of Plates by High Speed Projectiles. Presented at the 5th Midwestern Conference on Solid Mechanics, Michigan State University, East Lansing, Michigan, Sept. 1961.

3. Chou, Pei Chi: Visco-Plastic Flow Theory in Hypervelocity Perforation of Plates. Proceedings of the Fifth Symposium on Hypervelocity Impact, Vol. 1, pt. 1, Apr. 1962.

4. Kraus, H.: Two Dimensional Analysis of a Hypervelocity Impact Upon a Visco-Plastic Plate. Proceedings of the Sixth Symposium on Hypervelocity Impact, Volume III, Apr. 1963.

5. Chou, Pei Chi; Mortimer, Richard W.; and Llorens, Richard E.: A Parametric Study of the Hypervelocity Perforation of Viscoplastic Plates. Drexel Institute of Technology, DIT Rept. No. 125-3, Jan. 1963.

6. Bachshian, F. A.: Visco-Plastic Flow by Impact of a Cylinder Upon a Plate (in Russian), Priklad. Mat. Makh. 12, 1948-47.

7. Prager, William: Introduction to Mechanics of Continua. Ginn and Co., 1961, p. 136.

8. Collins, Rufus D., Jr.; and Kinard, William H.: The Dependency of Penetration on the Momentum Per Unit Area of the Impacting Projectile and the Resistance of Materials to Penetration. NASA TN D-238, 1960.

9. Jahnke, Eugene; and Emde, Fritz: Table of Functions with Formulae and Curves. Fourth ed., Dover Publications, 1945, p. 211.

10. McLachlan, N. W.: Bessel Functions for Engineers. List of Formula pages 157-172, Oxford, London, 1934.

11. Carslaw, H. S.; and Jaeger, J. C.: Conduction of Heat in Solids. 1st Ed., 2nd impression, Oxford University Press, 1950, pp. 380, 370-73.

12. Hartree, D. R.: Some Properties and Applications of the Repeated Integrals of the Error Function. Mem. and Proc. Manchester Lit. and Phil. Soc., vol. 80, 1935-36, pp. 85-102.

13. Kaye, J.: A Table of the First Eleven Repeated Integrals of the Error Function. J. Math. Phys., V. 34, 1955-56, pp. 119-125. (See also RMT 58, MTAC, V. 10, 1956, p. 176.)

14. Mechtly, E. A.: The International System of Units. Physical Constants and Conversion Factors. NASA SP-7012, 1964.

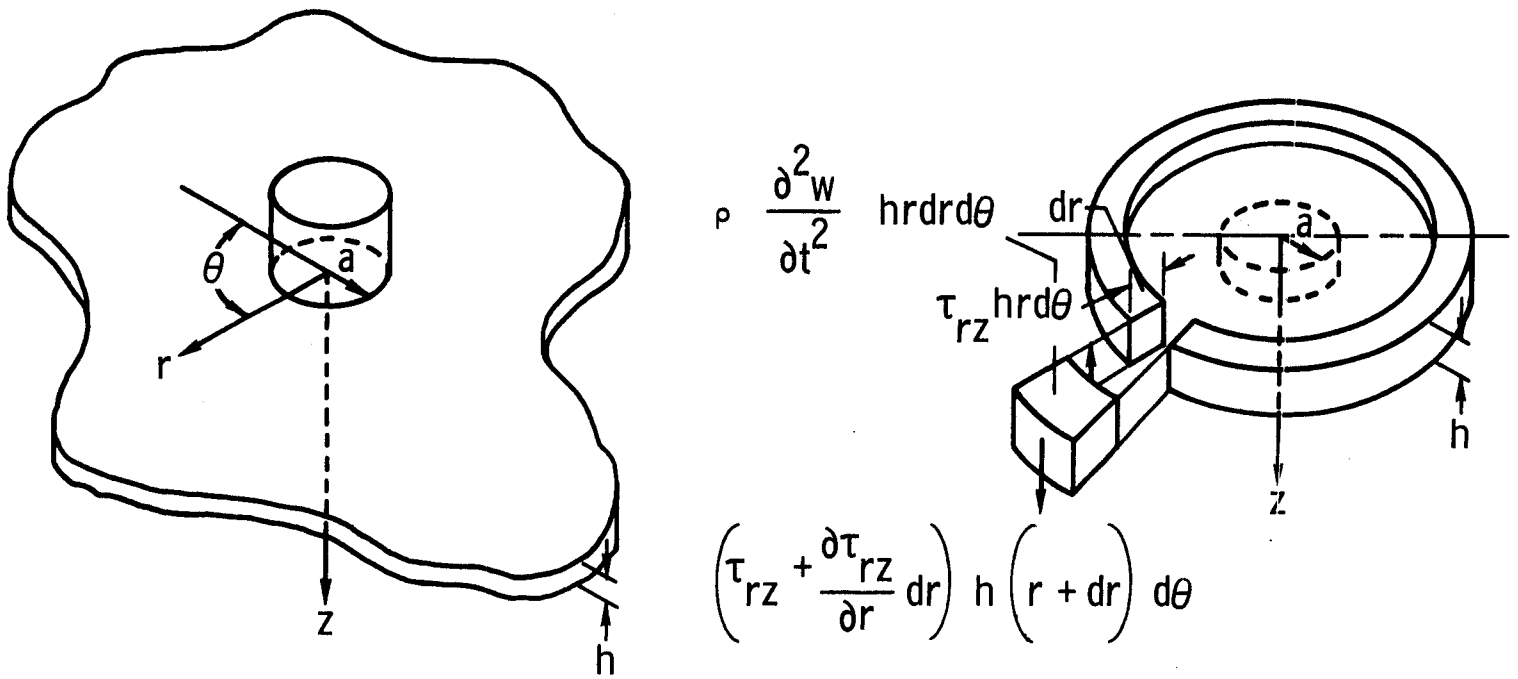

(a) Finite rigid projectile and infinite plate. (b) Circular ring element with equilibrium forces.

NASA

Figure 1.- Geometry and coordinate system of perforation.

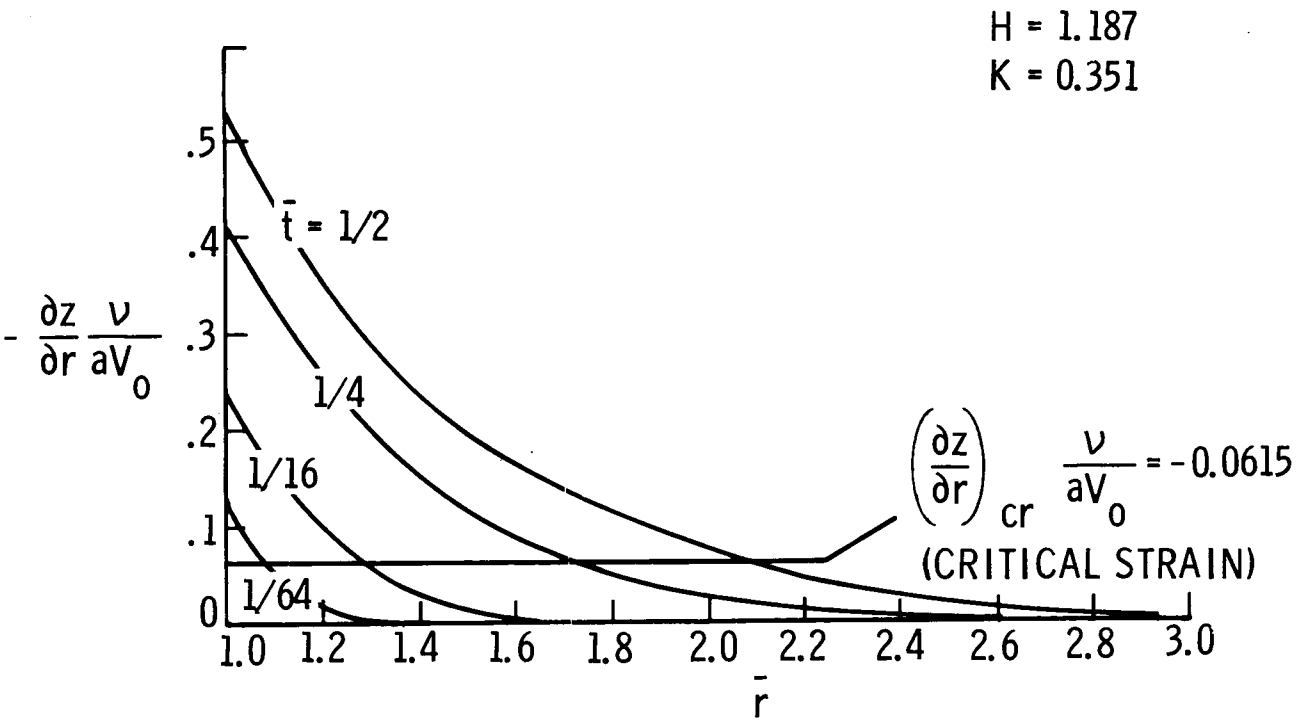

NASA

Figure 2.- Strain distributions for various times. h = 0.635 cm (1/4 in.); M_1 = 0.052 g; $\mu = 5\ \frac{kNs}{m^2}$ (0.05 megapoise); g_o = 1.2 km/s; $\rho = 2680\ \frac{kg}{m^3}$; a = 0.119 cm (3/64 in.); $k = 0.69\ \frac{GN}{m^2}$ (100 ksi).

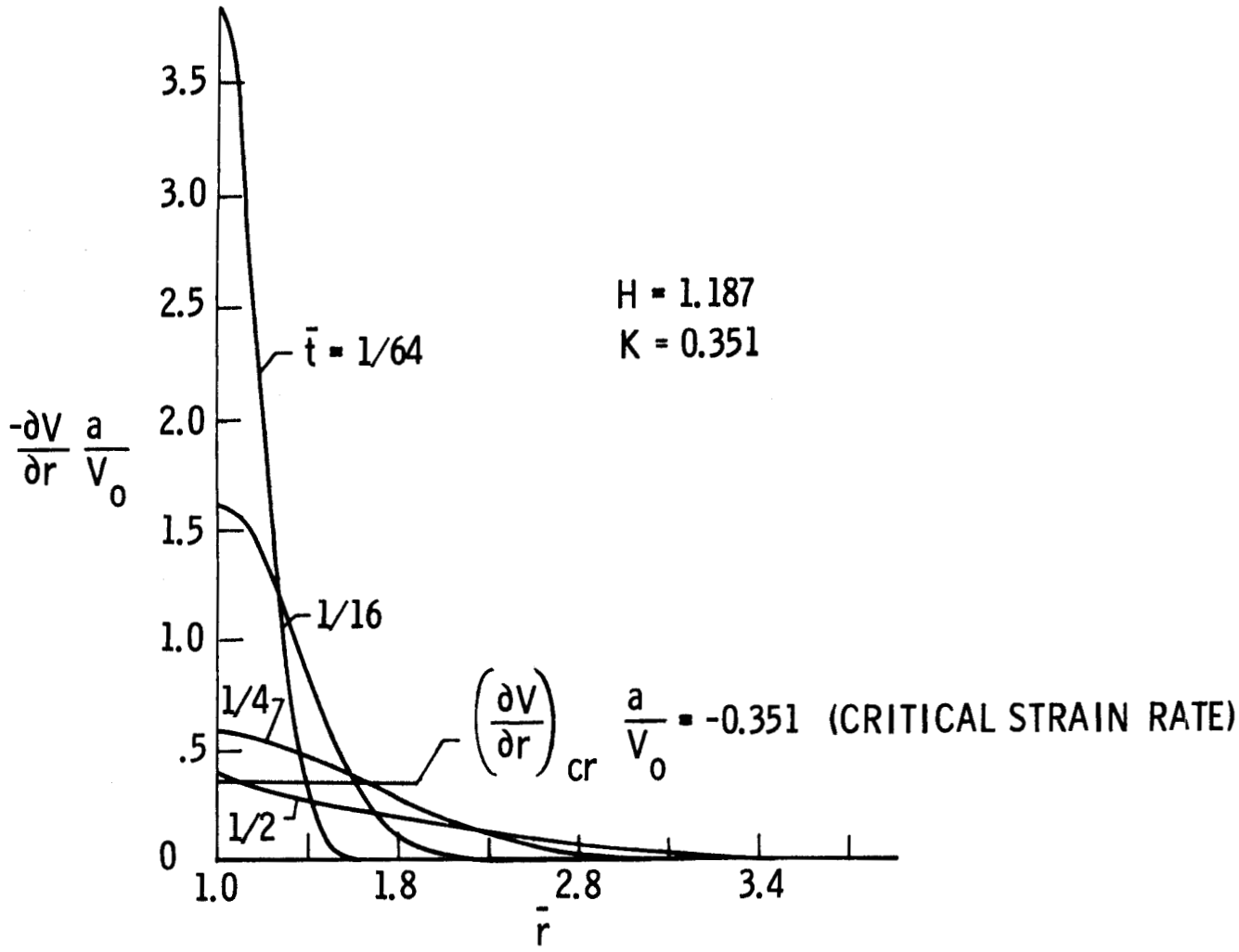

NASA

Figure 3.- Strain-rate distributions for various times. h = 0.635 cm (1/4 in.); M_1 = 0.052 g; g_o = 1.2 km/s; ρ = 2680 $\frac{kg}{m^3}$; a = 0.119 cm (3/64 in.); k = 0.69 $\frac{GN}{m^2}$ (100 ksi); μ = 5 $\frac{kNs}{m^2}$ (0.05 megapoise).

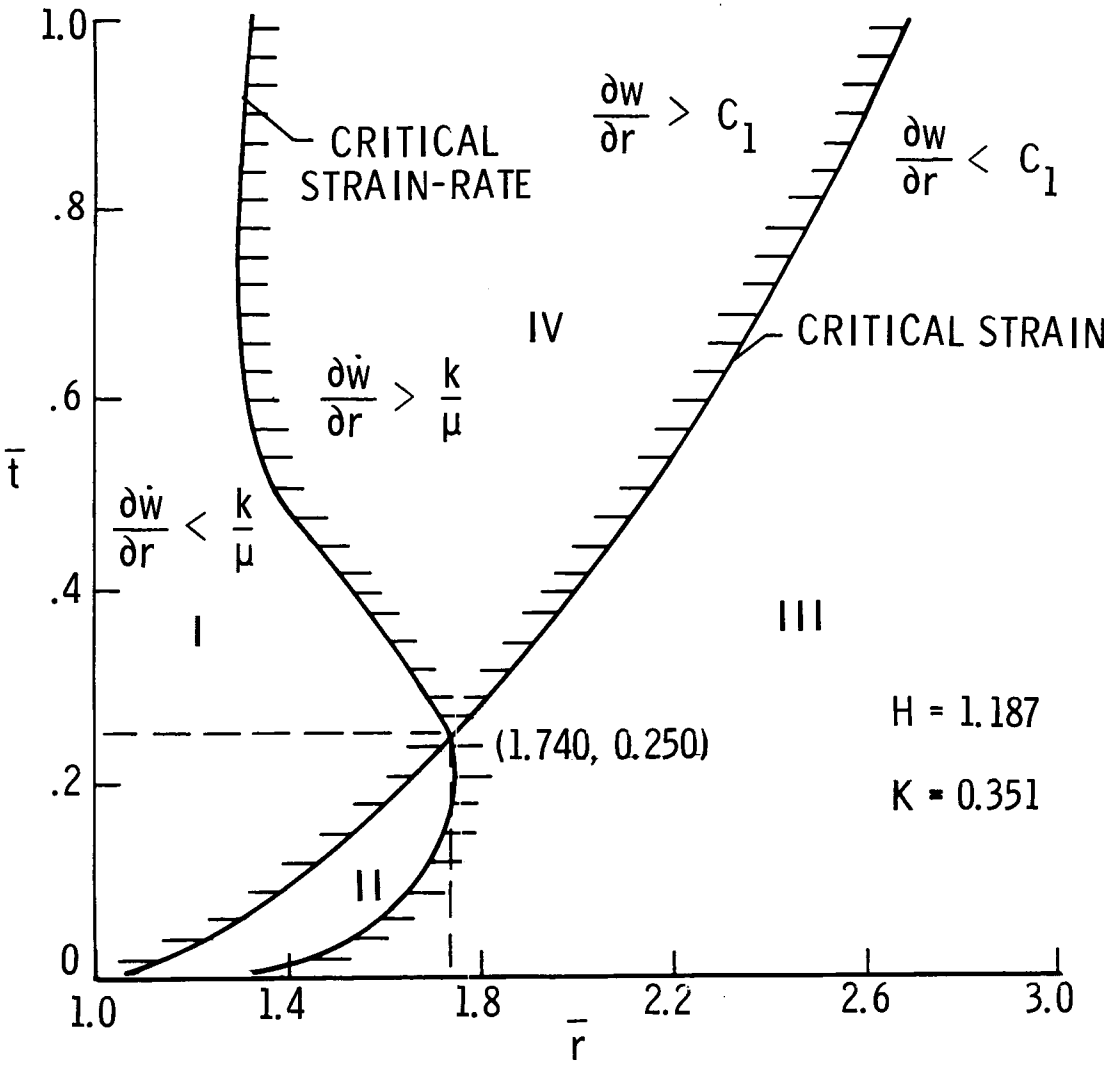

NASA

Figure 4.- Graphical representation for determining perforation radius and separation time. h = 0.635 cm (1/4 in.); M_1 = 0.052 g; $\mu = 5 \frac{kNs}{m^2}$ (0.05 megapoise); g_o = 1.2 km/s; $\rho = 2680 \frac{kg}{m^3}$; a = 0.119 cm (3/64 in.); $k = 0.69 \frac{GN}{m^2}$ (100 ksi).

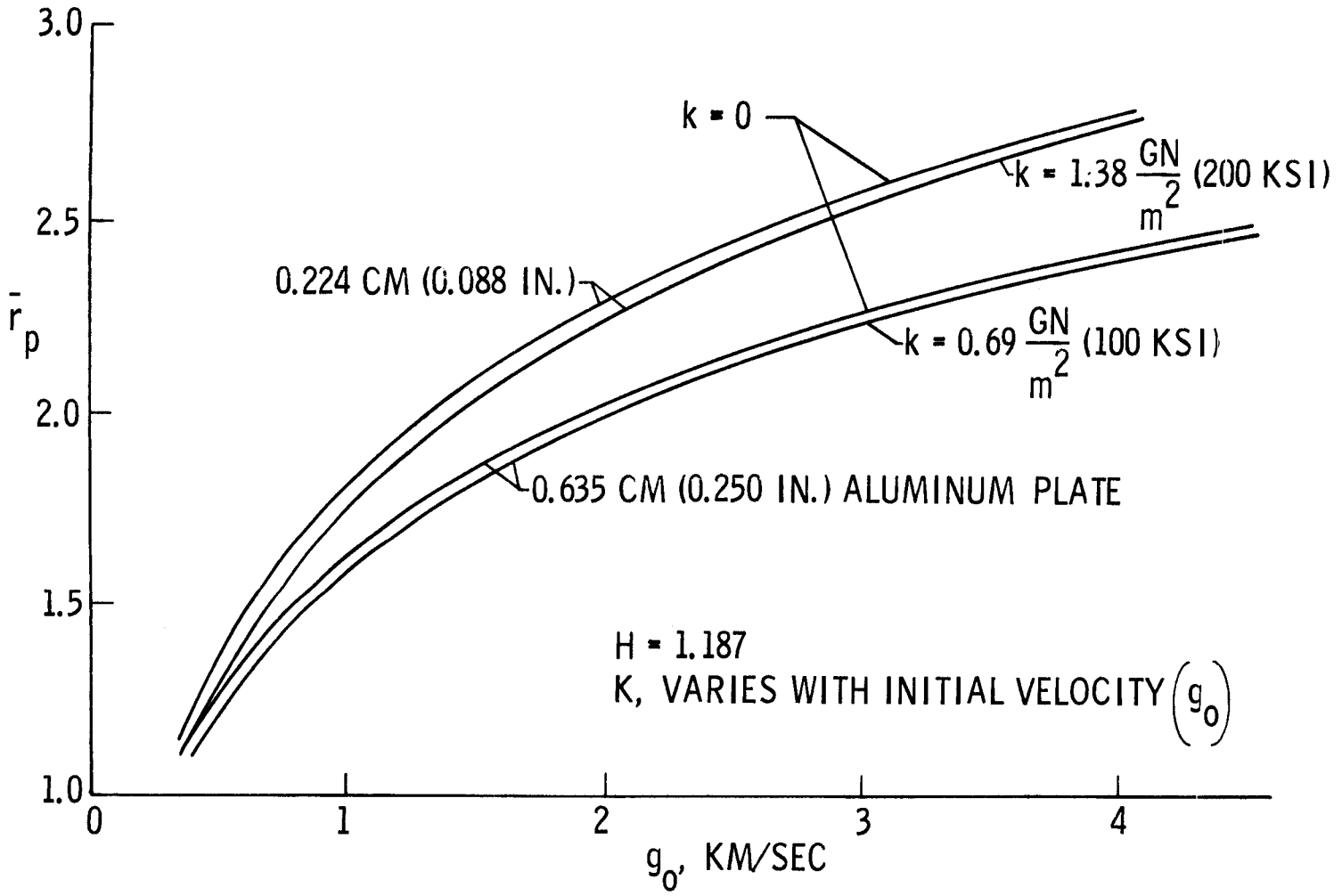

NASA

Figure 5.- Radius of perforation as a function of initial projectile velocity for steel and aluminum target plates of the same weight per unit area. M_1 = 0.052 g; a = 0.119 cm (3/64 in.); $\rho h = 17 \frac{kg}{m^2}$; $\mu = 5 \frac{kNs}{m^2}$ (0.05 megapoise).

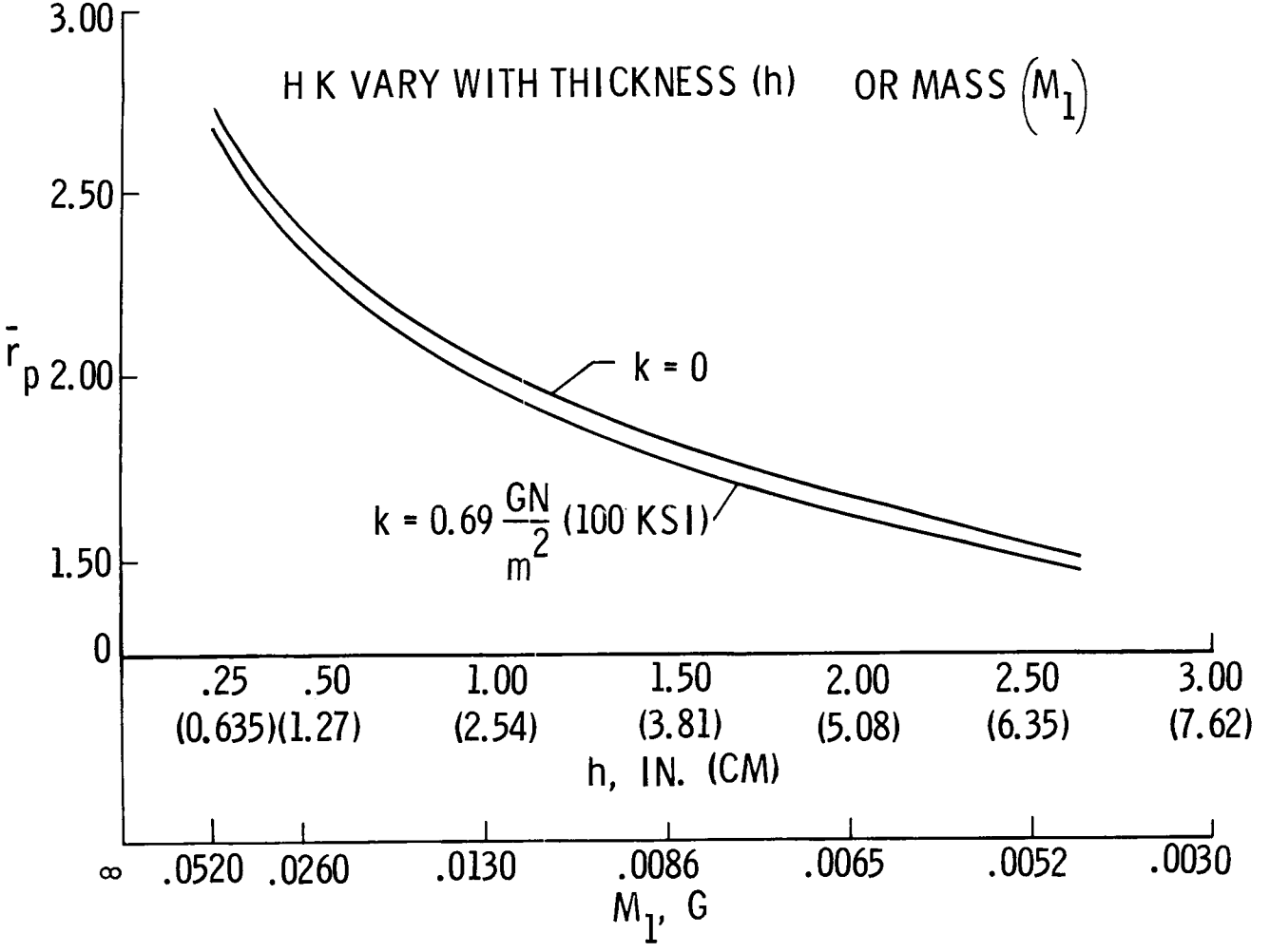

NASA

Figure 6.- Effect of variation in plate thickness or projectile mass on perforation radius. $\mu = 5 \frac{kNs}{m^2}$ (0.05 megapoise); $g_o = 6.096$ km/sec; $\rho = 2680 \frac{kg}{m^3}$; a = 0.119 cm (3/64 in.).

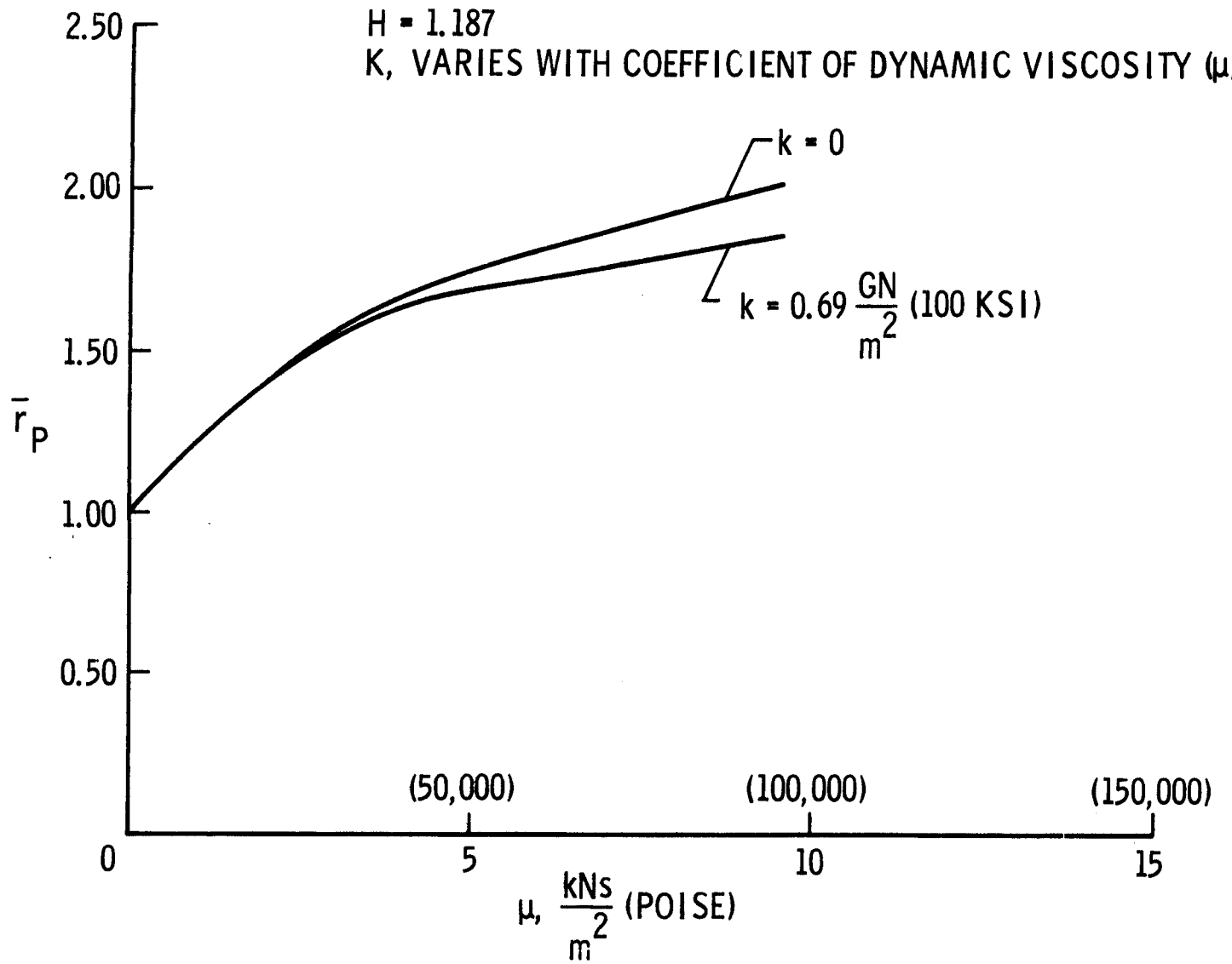

Figure 7.- Effect of variation in coefficient of dynamic viscosity on perforation radius. h = 0.635 cm (1/4 in.); M_1 = 0.052 g; g_o = 1.2 km/sec; ρ = 2680 $\frac{kg}{m^3}$; a = 0.119 cm (3/64 in.).

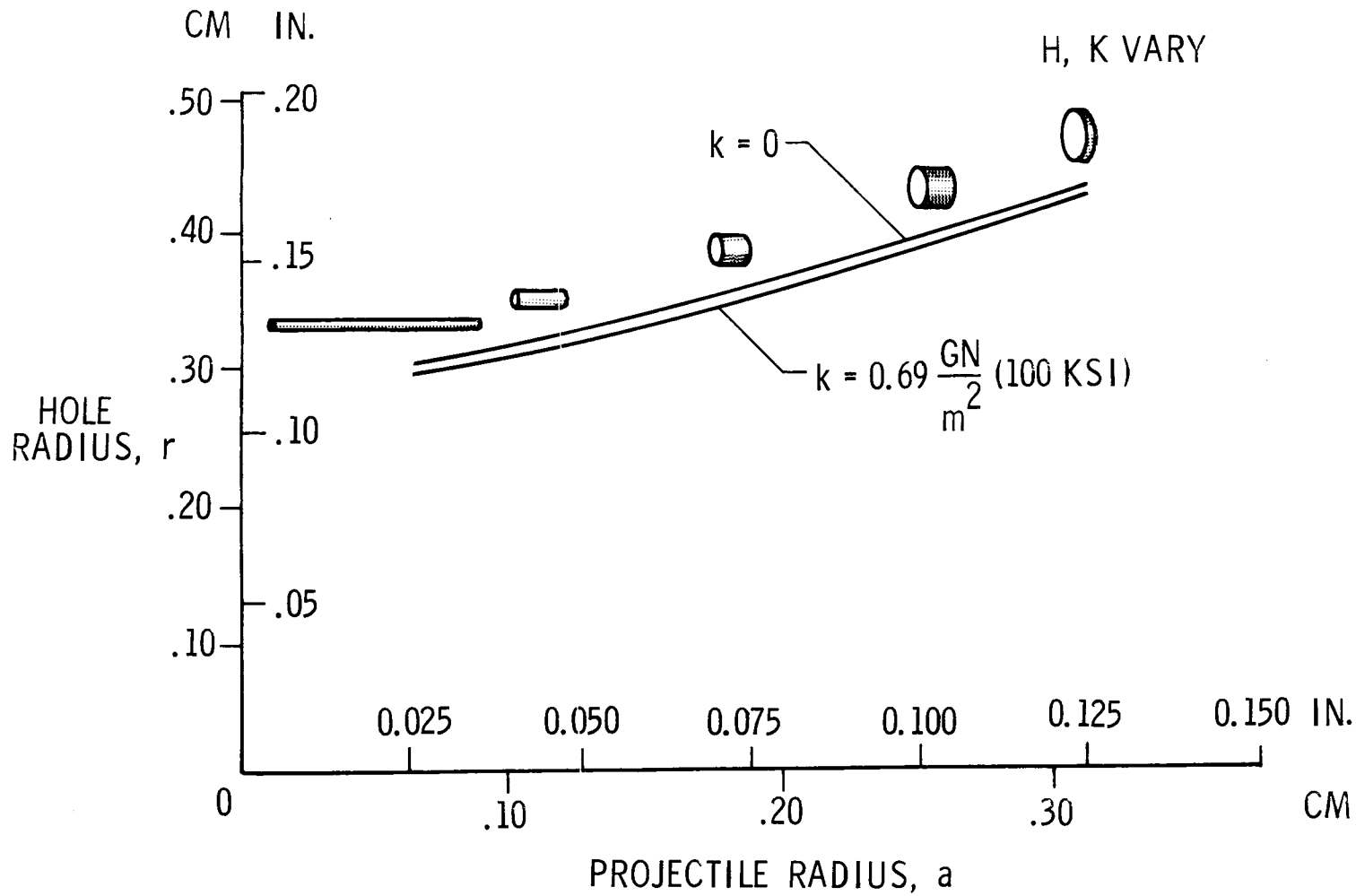

NASA

Figure 8.- Radius of perforation as a function of projectile radius. h = 0.635 cm (1/4 in.); M_1 = 0.052 g; $\mu = 5 \frac{kNs}{m^2}$ (0.05 megapoise); $\rho = 2680 \frac{kg}{m^3}$; g_o = 6.096 km/sec.

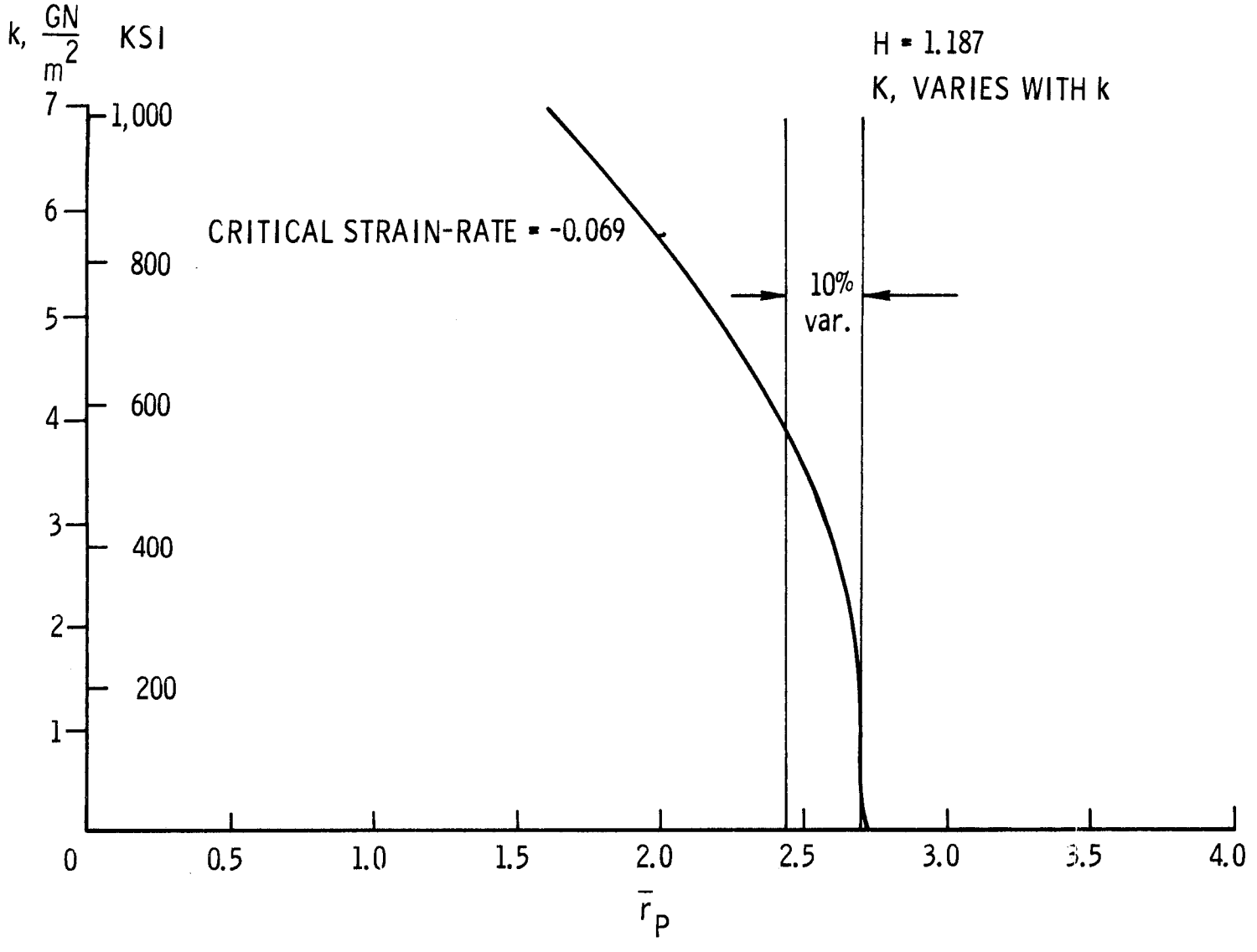

NASA

Figure 9.- Radius of perforation as a function of dynamic yield strength for a given separation criterion. h = 0.635 cm (1/4 in.); M_1 = 0.052 g; $\mu = 5 \frac{kNs}{m^2}$ (0.05 megapoise); $\rho = 2680 \frac{kg}{m^3}$; g_o = 6.096 km/sec; a = 0.119 cm (3/64 in.).

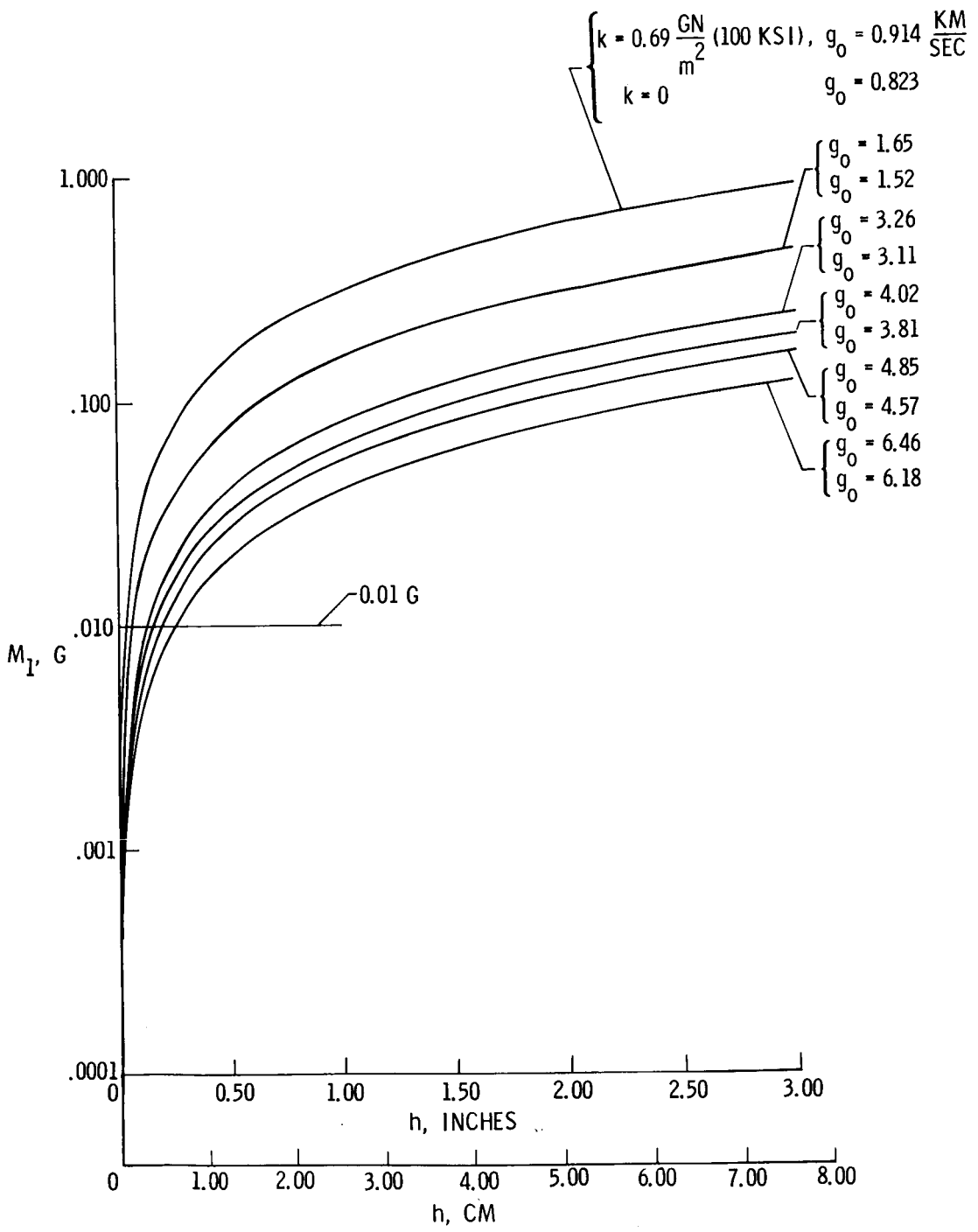

NASA

Figure 10.- Ballistic limit curves for projectile of 0.32 cm (1/8 in.) radius. $\mu = 5 \frac{kNs}{m^2}$ (0.05 megapoise); $\rho = 2680 \frac{kg}{m^3}$.

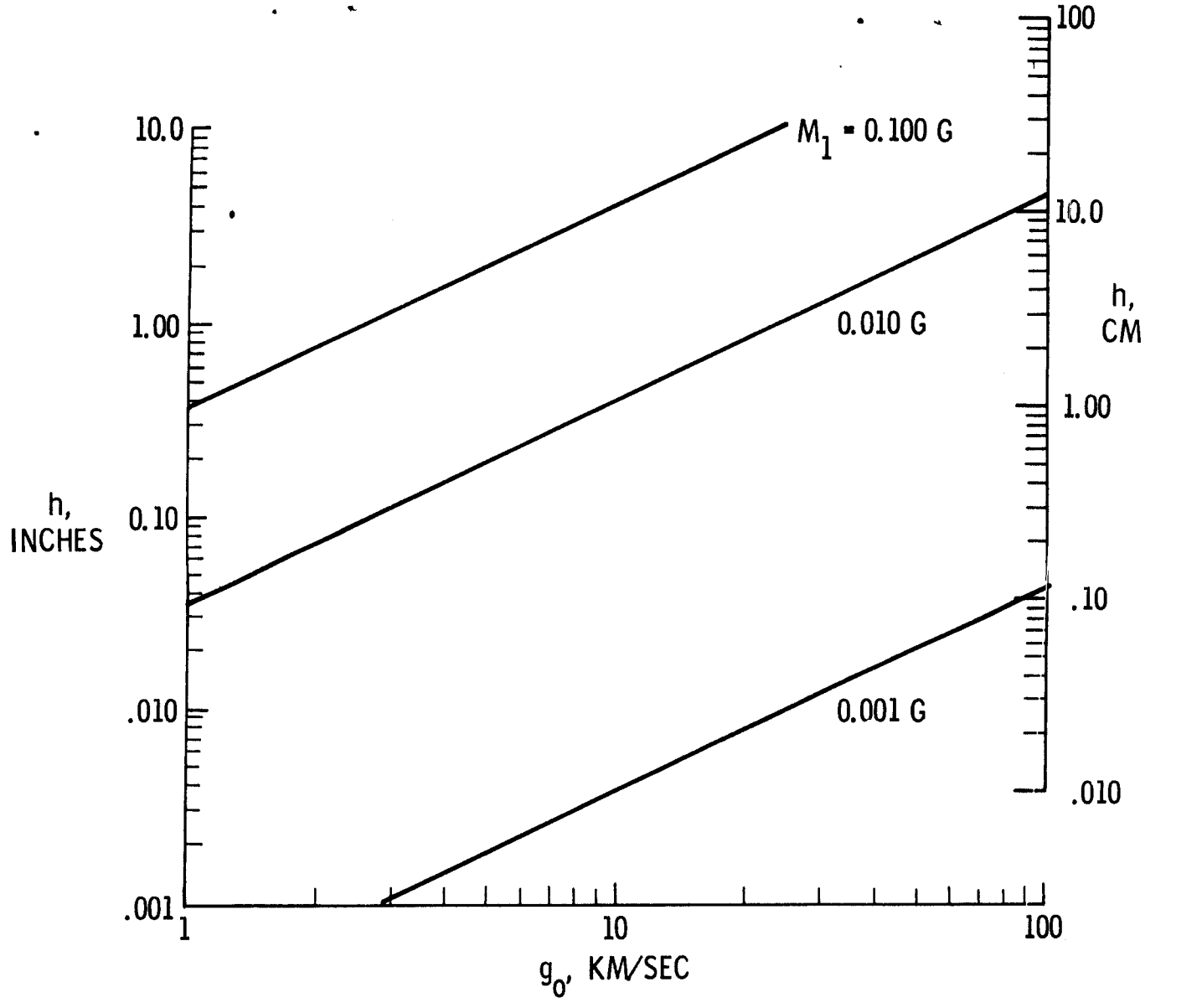

NASA

Figure 11.- Minimum plate thickness as a function of projectile velocity for projectiles of three different masses. $\mu = 5\ \frac{kNs}{m^2}$ (0.05 megapoise); $\rho = 2680\ \frac{kg}{m^3}$; $k = 0.69\ \frac{GN}{m^2}$ (100 ksi) a = 0.32 cm (1/8 in.).

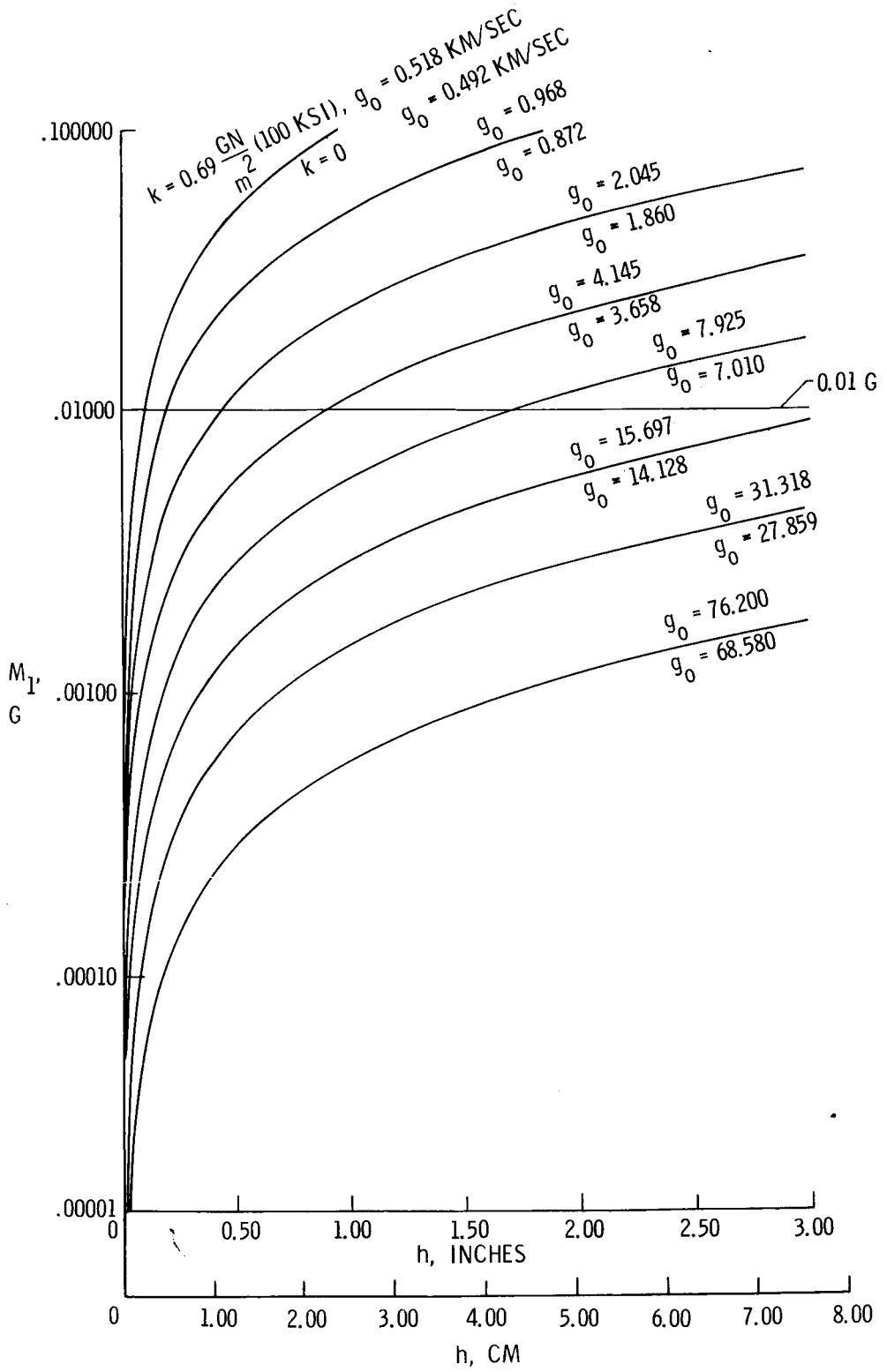

NASA

Figure 12.- Ballistic limit curves for projectile of 0.119 cm (3/64 in.) radius. $\mu = 5 \frac{kNs}{m^2}$ (0.05 megapoise); $\rho = 2680 \frac{kg}{m^3}$.

NASA-Langley, 1964